JACS JOURNAL OF THE AMERICAN CHEMICAL SOCIETY

Article

Cite This: J. Am. Chem. Soc. 2018, 140, 9758−9767

pubs.acs.org/JACS

Accelerating DNA-Based Computing on a Supramolecular Polymer

Wouter Engelen,[†,‡] Sjors P. W. Wijnands,[†] and Maarten Merkx*[,†,‡]

[†]Institute for Complex Molecular Systems, Eindhoven University of Technology, P.O. Box 513, Eindhoven 5600 MB, The Netherlands

[‡]Laboratory of Chemical Biology, Department of Biomedical Engineering, Eindhoven University of Technology, P.O. Box 513, Eindhoven 5600 MB, The Netherlands

Supporting Information

ABSTRACT: Dynamic DNA-based circuits represent versatile systems to perform complex computing operations at the molecular level. However, the majority of DNA circuits relies on freely diffusing reactants, which slows down their rate of operation substantially. Here we introduce the use of DNA-functionalized benzene-1,3,5-tricarboxamide (BTA) supramolecular polymers as dynamic scaffolds to template DNA-based molecular computing. By selectively recruiting DNA circuit components to a supramolecular BTA polymer functionalized with 10-nucleotide handle strands, the kinetics of strand displacement and strand exchange reactions were accelerated 100-fold. In addition, strand exchange reactions were also favored thermodynamically by bivalent interactions between the reaction product and the supramolecular polymer. The noncovalent assembly of the supramolecular polymers enabled straightforward optimization of the polymer composition to best suit various applications. The ability of supramolecular BTA polymers to increase the efficiency of DNA-based computing was demonstrated for three well-known and practically important DNA-computing operations: multi-input AND gates, Catalytic Hairpin Assembly and Hybridization Chain Reactions. This work thus establishes supramolecular BTA polymers as an efficient platform for DNA-based molecular operations, paving the way for the construction of autonomous bionanomolecular systems that confine and combine molecular sensing, computation, and actuation.

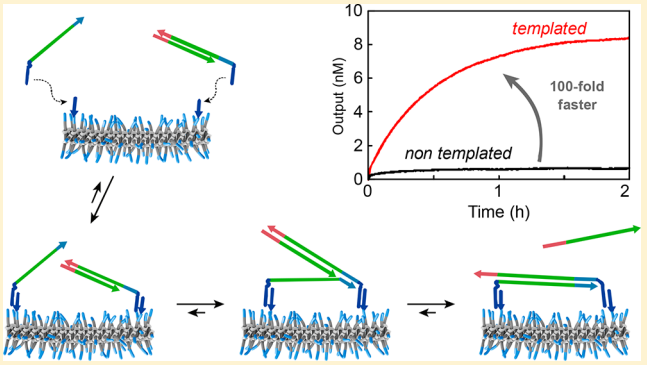

INTRODUCTION

In the past decade the detailed understanding of the kinetics and thermodynamics of oligonucleotide hybridization has led to the widespread implementation of DNA as a molecular construction material and information carrier.[1] Especially, the ability to design mechanistically identical, but orthogonal, modules solely based on the complementarity of oligonucleotide sequences allows the construction of (1) autonomous systems that emulate life-like feature such as oscillations[2] and traveling waves,[3] (2) molecular robots,[4,5] walkers[6−8] and machines,[9,10] and (3) networks inspired by traditional silicon-based circuits that perform binary operations and calculations at the molecular level.[11−16] Thus, far, the vast majority of DNA-circuits and networks are based on the interaction between freely diffusing oligonucleotide reactants. In order to avoid background and nonintended side reactions, DNA-based molecular circuits typically employ low nanomolar concentrations of individual reactants. As the reaction rates and thus the computing time are proportional to the absolute concentration of the reactants, these circuits operate slowly and can take many hours to days to complete calculations, hampering their translation into practical applications.

To decouple reaction rates from the absolute reactant concentration, nature uses molecular templates such as the cytoskeleton, cellular membranes, and hub-proteins to recruit network components, thereby increasing their effective concentration without increasing the total amount of molecules.[17−19] This principle of colocalizing reactants to enhance their association kinetics has also been employed in oligonucleotide-based systems using DNA-walkers immobilized on microparticles,[8,20] membranes,[21,22] and DNA origami scaffolded oligonucleotide circuits and logic operations.[23−29] Particularly, DNA origami provides the unique advantage of immobilizing oligonucleotide reactants at a predefined position on the scaffold with high precision, introducing spatial constrains in addition to chemical specificity as a means of orthogonality. However, immobilizing oligonucleotide reactants on a DNA origami scaffold requires careful positioning of the circuit components to facilitate efficient interaction between reactants. Additionally, circuits immobilized on static scaffolds are sensitive to assembly defects as non- or mis-incorporated reactants will terminate the propagation of the signal along the scaffold.[27,30,31] Because the probability of assembly defects increases with the circuit's complexity, the scalability of immobilized circuits therefore remains challenging. Other efforts to increase the kinetics of

Received: June 11, 2018
Published: July 10, 2018

DOI: 10.1021/jacs.8b06146
J. Am. Chem. Soc. 2018, 140, 9758−9767

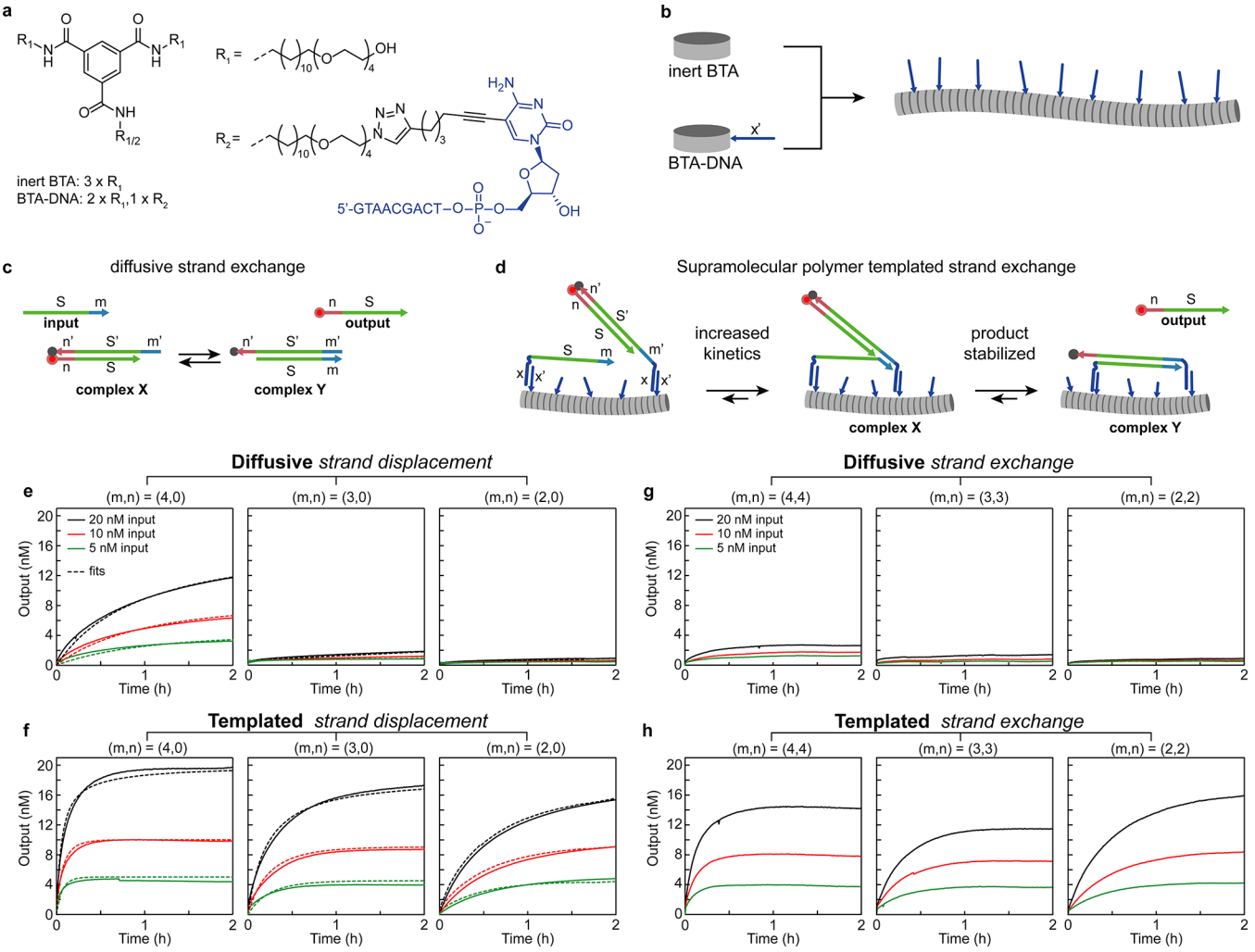

Figure 1. Principle of accelerating DNA circuits by a supramolecular polymer template. (a) Chemical structure of the inert and DNA-handle functionalized BTA monomers. (b) Supramolecular polymers decorated with DNA-handles are obtained by mixing desired ratios of inert BTA and BTA-DNA. (c) Mechanism of a strand exchange reaction using freely diffusing oligonucleotide reactants. (d) Principle of a BTA polymer templated strand exchange reaction. As the oligonucleotide reactants are elongated with an antihandle sequence they are recruited to the supramolecular polymer. This results in an increase in effective concentration and consequently increases the association kinetics of toehold binding. Additionally, as the final product is multivalently anchored to the supramolecular polymer, the product is stabilized, resulting in increased operation yields. (e) Kinetic characterization and fits of diffusive strand displacement ($n = 0$) with toeholds of 4, 3, and 2 nucleotides, yielding $k_{(4,0),D} = 1.54 \times 10^{-5}$ nM^{-1} s^{-1}, $k_{(3,0),D} = 5.36 \times 10^{-7}$ nM^{-1} s^{-1} and $k_{(2,0),D} = 1.88 \times 10^{-7}$ nM^{-1} s^{-1}. (f) The same strand displacement reactions templated on the BTA polymer, yielding $k_{(4,0),T} = 2.20 \times 10^{-4}$ nM^{-1} s^{-1}, $k_{(3,0),T} = 6.26 \times 10^{-5}$ nM^{-1} s^{-1} and $k_{(2,0),T} = 2.58 \times 10^{-5}$ nM^{-1} s^{-1}. (g) Kinetic characterization of diffusive strand exchange reactions with toeholds of identical lengths of 4, 3, and 2 nucleotides. (h) The same strand exchange reactions templated on the BTA polymer. Modifications of the base and output with a quencher and fluorophore, respectively allows the monitoring of the reaction by fluorescence. Experiments were performed in triplicate with 500 nM BTA-DNA, 4.5 μM inert BTA, 20 nM complex X and 5, 10, and 20 nM input in TAE/Mg^{2+} supplemented with 1 mg mL^{-1} BSA at 25 °C.

DNA strand displacement include the use of RecA as a protein-based catalyst and the use of cationic copolymers, which are postulated to enhance kinetics by stabilizing toehold complex formation.[32−34]

The potential of supramolecular polymers as dynamic, adaptable, and modular platforms for molecular signal processing has been widely recognized.[35−37] Here we introduce one-dimensional supramolecular polymers of benzene-1,3,5-tricarboxamide (BTA) as a generic, modular, and easy to implement platform to recruit and colocalize DNA-circuit reactants. We recently reported that BTA derivatives functionalized with 10 nucleotide long receptor strands (BTA-DNA) form remarkably stable, micrometer-long supramolecular polymers that allow efficient recruitment of DNA-functionalized proteins, promoting protein−protein complex formation 1000-fold by increasing their effective local concentration.[38] The supramolecular nature allows this polymer platform to dynamically adapt and remodel its nanoscopic composition, which avoids the need for tailor-made scaffold designs. First, we establish the effect of this supramolecular polymer scaffold on the kinetics and thermodynamics of two fundamental processes in DNA-computing, toehold-mediated strand displacement and strand exchange reactions. Next, the ability of supramolecular BTA scaffolds to accelerate three well-known and practically important DNA-computing operations is explored: multiple input AND gates, catalytic hairpin assembly (CHA), and the hybridization chain reaction (HCR). The BTA-templated HCR is also monitored using super resolution fluorescence micros-

DOI: 10.1021/jacs.8b06146
J. Am. Chem. Soc. 2018, 140, 9758−9767

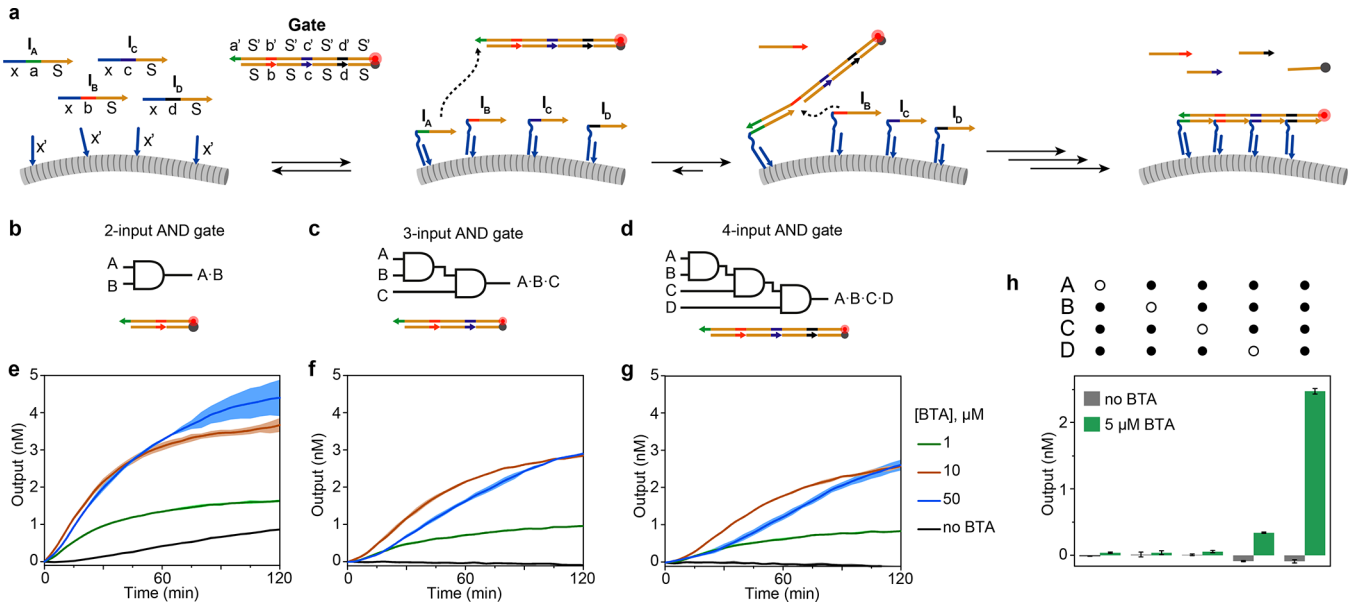

Figure 2. BTA polymer templated multi-input AND gates. (a) Mechanism of a templated four-input AND gate, based on sequential strand displacement reactions. All input strands are elongated with a 10 nucleotide antihandle that is complementary to the handle strands on the BTA polymer, facilitating their recruitment to the supramolecular platform. (b–d) Schematic representation and DNA-based implementation of a two-, three-, and four-input AND gate, respectively. (e–g) Kinetic characterization of two-, three-, and four-input AND gates, respectively, at varying BTA concentrations containing 10% BTA-DNA. The negative slopes observed for the three- and four-input AND gates in the absence of BTA are probably due to bleaching of background fluorescence. (h) Response of the four-input AND gate to different combinations of input oligonucleotides. Shaded areas and error bars represent SEM of duplicate measurements. Experiments were performed with 10 nM Gate and 5 nM of each input in TAE/Mg^{2+} supplemented with 1 mg mL^{-1} BSA at 25 °C.

copy, allowing direct visualization of the BTA-templated HCR reaction product.

RESULTS AND DISCUSSION

Supramolecular Polymer Design. Figure 1a shows the structures of the benzene-1,3,5-tricarboxamide (BTA) derivatives used in this study. The self-assembly of BTA into micrometer-long polymers is governed by intermolecular 3-fold hydrogen bonding and hydrophobic interactions of the BTA core. The three amphiphilic dodecyl-PEG_4 side-arms shield the hydrogen bonds from water while facilitating water solubility of the assembled polymer.[39] The dynamic properties of the BTA polymers have been extensively studied by ensemble FRET measurements, super-resolution microscopy and hydrogen–deuterium exchange experiments, revealing dynamic exchange of BTA monomers at the hour time scale.[40,41] To recruit DNA-circuit reactants to the supramolecular polymer, a monomer functionalized with a 10 nucleotide long handle-oligonucleotide (BTA-DNA, 5′-GTAACGACTC$_{alkyne}$-3′) on one of its three arms was synthesized via a copper catalyzed cycloaddition reaction. Stable supramolecular polymers decorated with a range of handle-strand densities could be readily obtained by premixing different ratios of DNA-functionalized and inert BTA monomers (Figure 1b).[38] Our previous work also showed that the 10 nucleotide handle provides sufficient recruitment of complementary sequences at low nM concentrations, while also allowing rapid migration of the complementary antihandles via reversible association and dissociation.[38]

BTA-Templated Strand Displacement Reactions. Toehold mediated strand displacement and strand exchange reactions are fundamental reactions in DNA-based molecular computing (Figure 1c). In these reactions, an input DNA strand binds with toehold **m** to a single-stranded overhang on a double stranded substrate complex X and subsequently invades the duplex via branch migration to displace the output oligonucleotide. When the input fully invades the double stranded substrate (i.e., toehold **n** = 0, hereinafter termed *Strand Displacement*), the reaction is effectively irreversible and reaches quantitative conversion. When complex X contains base pairs that are not invaded by the input (i.e., toehold **n** > 0, hereinafter termed *Strand Exchange*), these base pairs have to spontaneously dissociate to release the output from the base strand, resulting in the activation of toehold **n′** on complex Y. Consequently, the reversed reaction can take place where the output rebinds with toehold **n** to complex Y and displaces the input from the base strand. As a result, complex X and complex Y coexist in an equilibrium that is dependent on the relative binding affinities of the two toeholds.

In order to recruit the DNA strand exchange reactions to the supramolecular polymer, the base strand of complex X was elongated at its 5′-end with a T_5 linker and a 10 nucleotide antihandle sequence (**x**) complementary to the handle oligonucleotide (**x′**) on the BTA-DNA monomer. Similarly, the input strand was also functionalized with a 5′ antihandle sequence (Figure 1d). To monitor the strand exchange reactions in real-time, the output strand was modified with a 5′ fluorophore while the base strand of complex X was modified with a quencher. Hence, when displaced from the base strand the output generates a stoichiometric increase in fluorescence intensity. All reactions were done using a 10% BTA-DNA to BTA ratio, as this density was shown in our previous work to provide a high effective concentration of the recruited proteins, while avoiding steric hindrance at higher BTA-DNA densities.[38] Figure 1e,f shows fluorescence kinetics experiments of diffusive (i.e., nontemplated) and BTA-templated strand displacement

DOI: 10.1021/jacs.8b06146
J. Am. Chem. Soc. 2018, 140, 9758–9767

reactions with 20 nM complex X and 5, 10, and 20 nM input and **m** = 4, 3, or 2 nucleotides, respectively. When the strand displacement reaction relies on freely diffusing reactants, the displacement kinetics display a strong dependency on the length of toehold **m**. In accordance with earlier work, diffusive strand displacement was found to be very slow for 2 and 3 nucleotide toeholds at low nM concentrations (Figure S2).[42] However, the same reaction was strongly accelerated in the presence of the BTA polymer template. Fitting of the experimentally obtained kinetic data using Visual DSD (Dynamic Strand Displacement) yielded a rate enhanced by 2 orders of magnitude for the 2 and 3 nucleotide toehold, whereas the rate enhancement with a toehold of 4 nucleotides was ∼14-fold.[43] The 100-fold increase in rate constant is consistent with the increased effective concentration of the DNA-strands on the BTA polymer, which can be estimated to be in the low μM range.[38] The smaller, 14-fold enhancement observed for the 4 nucleotide toehold suggests that in this case the rate of the templated displacement reaction may have become partially limited by the initial binding of the DNA components to the supramolecular scaffold and/or the dynamics of strand reorganization along the supramolecular polymer.

Subsequently, fluorescence kinetics experiments were performed with strand exchange reactions that harbor toeholds of identical lengths (i.e., (**m**,**n**) = (4,4), (3,3) and (2,2), Figure 1g,h). Similar to strand displacement reactions, strand exchange is slow when relying on diffusive reactants at low nanomolar concentrations, but strongly accelerated when templated on the supramolecular BTA polymer (Figure S3). At least for (**m**,**n**) = (4,4), the strand exchange reaction reaches equilibrium both in the absence and presence of template, allowing assessment of the thermodynamic stabilization offered by the BTA polymer. Even though the length and GC content of toehold **m** and **n** are similar, the equilibrium of the diffusive strand exchange reaction is biased toward the initial state, showing formation of only 2 nM output upon reaction of 10 nM input with 20 nM complex X. This bias is probably due to a stabilizing effect of the fluorophore-quencher pair on toehold **n**.[44] In contrast, when templated, the same reaction yields 8 nM output strand, showing that the supramolecular BTA polymer stabilizes the formed product due to multivalent interactions with the polymer template.

Multi-input AND Gates. Because of their sequential nature, multi-input AND gates based on cascaded strand exchange reactions are notoriously slow, making AND gates beyond 2-inputs very inefficient. To challenge the effectiveness of supramolecular templating, we implemented our BTA polymer scaffold to promote two-, three-, and four-input AND gates (Figure 2). Here, input A (I_A) binds to a toehold (**a′**) on the gate and displaces a blocking strand (**S-b**), hereby activating the downstream toehold (**b′**) on the gate. Subsequently, input B (I_B) is able to bind to this toehold and displace the second blocking strand from the gate. For a two-input AND gate, this second blocking strand is modified with a quencher to quench a fluorophore present on the base strand of the gate (Figure 2b). For a three- and four-input AND gate this process is extended with one or two additional strand exchange reactions (Figure 2c,d). Hence, only when all input oligonucleotides are present the cascade is completed and the quencher is displaced from the fluorophore. In order to template the multi-input AND gates on the supramolecular BTA polymer, the input strands were elongated on their 5′ ends with the 10 nucleotide antihandle sequence (**x**) complementary to the handle oligonucleotide (**x′**) on the supramolecular polymer. Consequently, the first strand exchange reaction results in anchoring of the gate to the supramolecular polymer platform. Figure 2e−g shows the activation of the two-, three-, and four-input AND gate in time in the presence of varying amounts of supramolecular polymer containing 10% BTA-DNA. In absence of the polymer platform, only the two-input AND gate shows a slow increase in fluorescence output, whereas the three- and four-input AND gates show no detectable fluorescence increase at all over the 2 h incubation time. In contrast, all the AND gates are efficiently executed when templated on the BTA polymer. Following a short lag phase of 5−10 min, fluorescence rapidly increased for both the three- and four-input AND gates. This remarkable efficiency can be explained by the 100-fold rate increase for each DNA exchange reaction and the additional thermodynamic stabilization of the reaction product by multivalent interactions with the BTA polymer. The similar kinetic profiles suggest that the first strand exchange reaction, which is not templated by the BTA polymer but results in anchoring of the gate to the supramolecular polymer, has a large effect on the overall kinetics of these AND gates.

For a templated reaction, the kinetics and yield of the reaction are expected to depend on the amount of supramolecular scaffold. This is indeed what is observed, as there is a strong correlation for all three AND gates between the amount of output generated and the amount of polymer template, for BTA concentrations up to 5 μM (Figure S4). Whereas increasing the BTA concentration beyond 10 μM does not further increase the reaction yield, the kinetics of the reaction are affected. This effect is most clearly apparent for the three- and four-input AND gates, where increasing the BTA concentration increases the lag phase. As the downstream strand exchange reactions require the alignment of the downstream inputs via their migration along the polymer backbone, the strands have to migrate over a longer distance to allow toehold association which slows down the downstream strand exchange reactions. Consequently, the overall optimum in BTA polymer concentration can be qualitatively explained by a trade-off between a sufficiently large polymer surface to accommodate all AND-gate products, and the inversely correlated effective concentration of the input strands anchored to the supramolecular polymer. A similar optimum in BTA concentration was previously observed when studying the BTA polymer templated assembly of an enzyme−inhibitor pair.[38]

Though increasing the effective concentration of input oligonucleotides dramatically increases the efficiency of multiple input AND gates, this enhanced local concentration could also result in background activation of the AND gates. We therefore tested the robustness of the BTA-templated four-input AND gate by systematically omitting one of the input oligonucleotides. Even though the branch migration domains of all inputs are identical, no or only minimal background activation was observed when a single input is omitted (Figure 2h). Taken together, these results show that the efficiency of multiple-input AND gates can be enhanced over many orders of magnitude by simply templating them on the supramolecular BTA polymers, without a need for sequence optimization to suppress background activation.

Catalytic Hairpin Assembly. First reported by Yin et al., Catalytic Hairpin Assembly (CHA) is an enzyme-free, isothermal amplification strategy based on the catalytic formation of a duplex from two metastable hairpin structures, initiated by a single-stranded catalyst oligonucleotide.[45,46] As

DOI: 10.1021/jacs.8b06146
J. Am. Chem. Soc. 2018, 140, 9758−9767

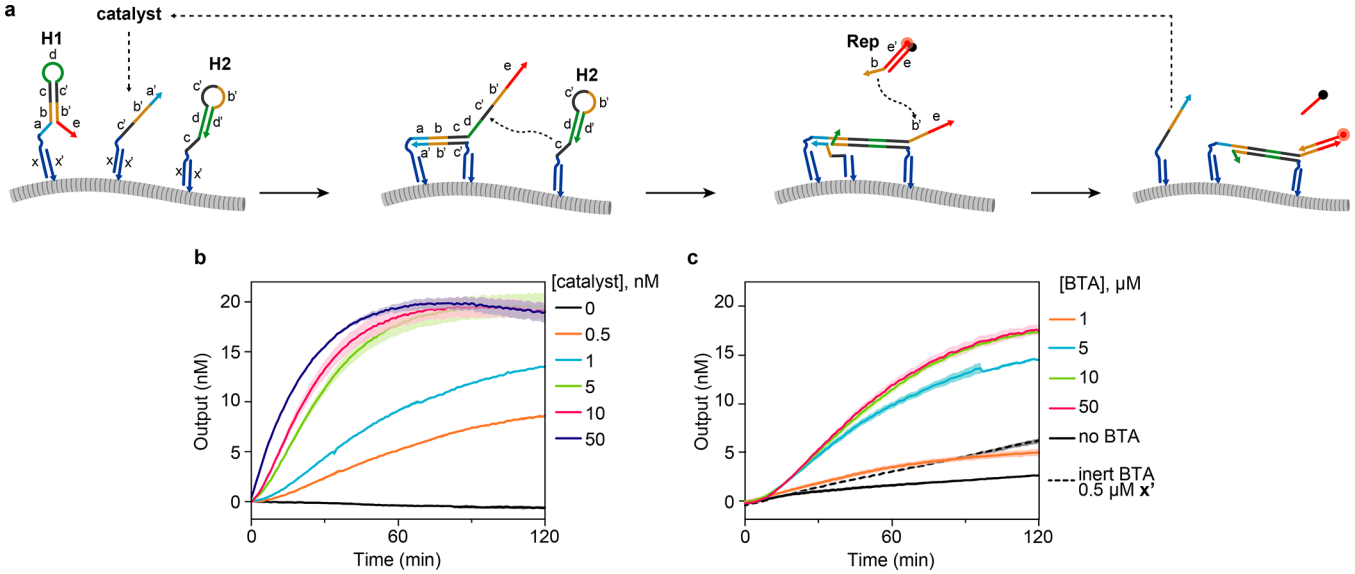

Figure 3. Supramolecular polymer templated Catalytic Hairpin Assembly (CHA). (a) Mechanism of a BTA templated CHA, based on the catalytic formation of a duplex from two metastable hairpins (H1 and H2). Opening of H1 by the catalyst results in activation of toeholds **b′** and **c′**, consequently allowing H2 to bind and invade the H1:catalyst duplex. The catalyst is spontaneously released from the unstable ternary H1:catalyst:H2 complex to complete the catalytic cycle. The CHA is monitored in real time by measuring the fluorescence intensity of a reporter duplex that is displaced by the opened H1. To template the CHA on the BTA polymer, all oligonucleotide reactants are elongated with a handle sequence at their 5′ ends. (b) Kinetic characterization of the CHA templated on the BTA polymer (5 μM, 10% BTA-DNA) initiated by different concentrations of catalyst. The negative slope observed in the absence of catalyst, is probably due to bleaching of background fluorescence. (c) Kinetic characterization of the CHA templated on various BTA concentrations containing 10% BTA-DNA directly after adding 1 nM catalyst. Shaded areas represent SEM of duplicate measurements. Experiments were performed with 20 nM H1, 100 nM H2, and 20 nM Rep in TNaK buffer supplemented with 1 mg mL^{-1} BSA at 37 °C.

CHA is based on the interaction between freely diffusing substrate hairpins, we envisioned that colocalizing the reactants on our supramolecular polymer platform could significantly increase the rate of CHA. In CHA, the catalyst binds to toehold **a** on the initial hairpin (H1), resulting in opening of the hairpin via branch migration and activation of toeholds **b′** and **c′** on H1. Toehold **c′** on the opened H1 allows the second hairpin (H2) to bind, followed by invasion of the H1:catalyst duplex by H2, resulting in the formation of an unstable ternary complex. When the catalyst dissociates from the ternary complex, the catalyst can bind to a new H1 and initiate another catalytic cycle. The progress of the CHA reaction can be monitored using a reporter duplex that is activated by binding to toehold **b′** on the H1:H2 duplex product. In order to template the CHA reaction on the supramolecular BTA polymer, all oligonucleotide reactants were elongated with the antihandle sequence at their 5′ ends (Figure 3a). First, the performance of the CHA with 20 nM H1, 100 nM H2, and 20 nM Rep was evaluated at different concentrations of catalyst in the presence of 5 μM BTA polymer, containing 10% BTA-DNA. Figure 3b shows that recruiting the metastable hairpins on the supramolecular polymer does not introduce spurious side-reactions as no background increase in fluorescence is observed in absence of catalyst. Next, the addition of catalytic concentrations of catalyst results in a rapid increase in fluorescence intensity which is correlated to the catalyst concentration. Importantly, even with a catalyst concentration as low as 0.5 nM, half of the substrate H1 is activated within 2 h, representing a turnover of ~10 h^{-1} under these experimental conditions. This result shows that the catalyst can still dissociate from the intermediate ternary complex, even though this complex is stabilized by the supramolecular polymer.

Next, the dependence of the CHA reaction on the amount of BTA polymer was evaluated by monitoring the reaction using 1 nM catalyst and maintaining 10% BTA-DNA (Figure 3c). In the absence of supramolecular polymer, CHA is inefficient as only a gradual increase in fluorescence in time is observed. After an initial lag phase, CHA is up to an order of magnitude faster when templated by the BTA polymer. At low BTA concentrations, the templated CHA is clearly correlated to the total amount of BTA. In contrast to recruitment of the multi-input AND gates, the speed of the CHA does not decrease at high BTA concentrations, suggesting that the dissociation of the catalyst from the ternary complex is rate limiting, rather than the association kinetics between H1 and H2. Interestingly, a minor increase in CHA activation is also observed for a control reaction that contains 5 μM inert BTA polymer and 500 nM nonconjugated handle. This is most likely caused by weak, alternative conformations of the **c′** domain of the catalyst when the antihandle is not hybridized to the complementary handle oligonucleotide, hampering the CHA in absence of the handle (Figure S5). Though the presence of this alternative conformation was not intended, this could provide an interesting strategy to further reduce background activation of the CHA. Finally, the performance of the CHA was monitored in the presence of different concentrations of BTA polymer, while ensuring a constant total concentration of BTA-DNA, yielding polymers with different handle densities (500 nM BTA-DNA, 0.166−9.5 μM inert BTA). Figure S6 shows that the performance of the CHA reaction is optimal using 5−10% BTA-DNA. The decrease observed at higher BTA-DNA to BTA ratios could be due to steric hindrance and/or a decrease in total polymer surface area.

Hybridization Chain Reaction. The Hybridization Chain Reaction (HCR), first introduced by Pierce and co-workers, is a widely established amplification strategy used in molecular diagnostics and imaging of nucleic acids.[47−50] HCR is based on

DOI: 10.1021/jacs.8b06146
J. Am. Chem. Soc. 2018, 140, 9758−9767

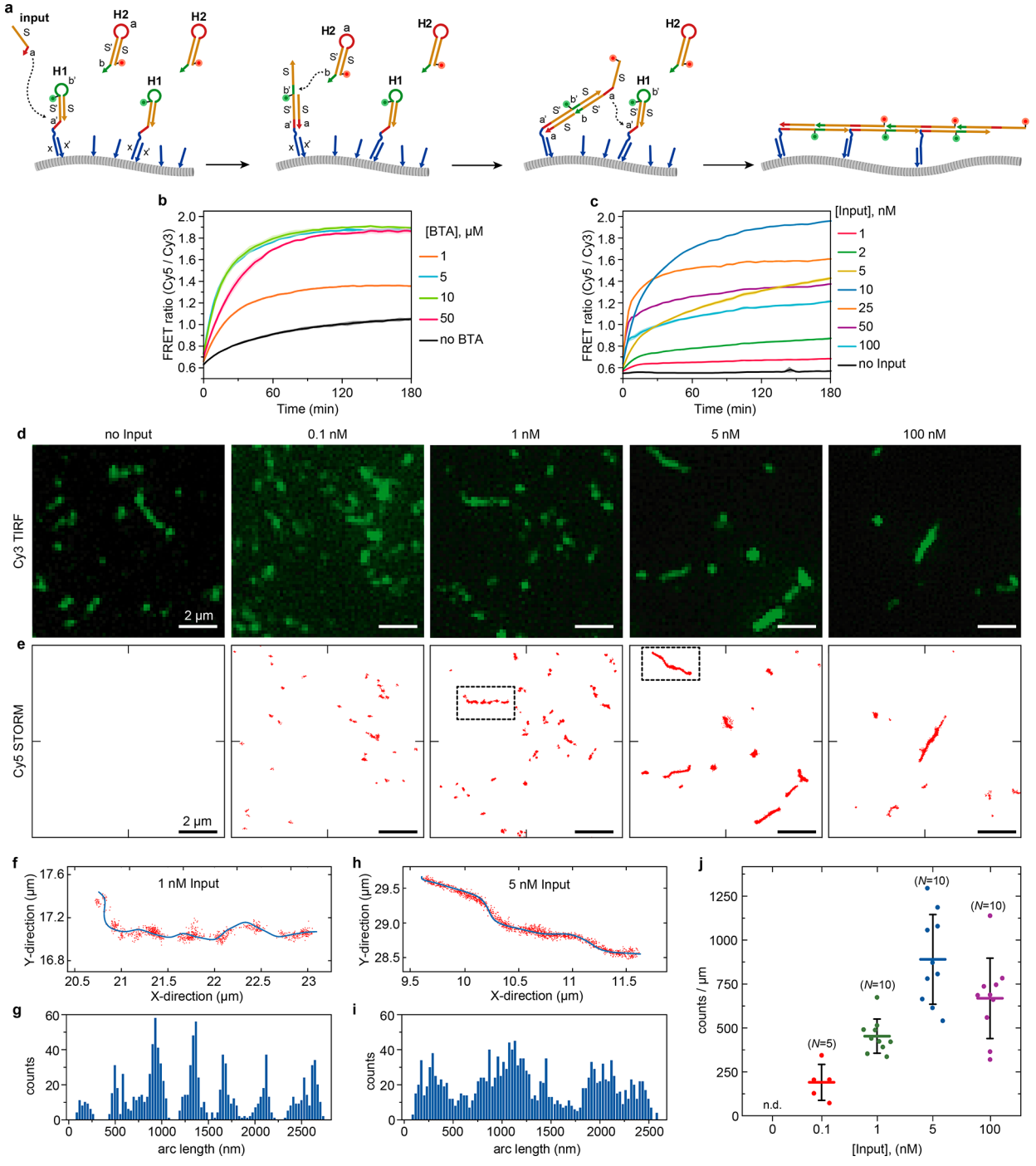

Figure 4. Supramolecular polymer templated Hybridization Chain Reaction (HCR). (a) Mechanism of BTA-templated HCR, based on the alternating assembly of two metastable hairpins (H1 and H2). H1 is anchored to the BTA polymer by extending its 5′-end with an antihandle sequence. The input binds to toehold **a′** on H1 and opens the hairpin via branch migration, resulting in activation of toehold **b′**. H2 subsequently binds to the activated toehold **b′** and is invaded by H1. This results in the activation of toehold **a′**, which allows a new H1 to bind, resulting in a chain reaction of assembling alternating hairpins. The HCR is monitored by measuring FRET between a donor (Cy3) in H1 and an acceptor (Cy5) on H2. (b) HCR kinetics templated on various BTA concentrations containing 10% BTA-DNA directly after adding 10 nM input. (c) HCR kinetics templated on the BTA polymer (5 μM, 10% BTA-DNA) using different input concentrations. Shaded areas represent SEM of duplicate measurements. (d) Cy3 TIRF imaging of decorated BTA polymers immobilized on glass coverslips. The Cy3 labeled H1 is used to image the supramolecular polymer backbone. (e) Super-resolution imaging using STORM of the HCR product templated on the supramolecular polymer. As H2 is only recruited to the polymer when incorporated in the HCR product, H2 is used to represent the HCR product. (f) Traced BTA polymer backbone from the boxed cluster in (e), initiated by 1 nM input. (g) Histogram representing number of Cy5 localizations along the traced polymer backbone (Binsize = 50 nm). (h,i) Similar as panels f and g but for the boxed cluster shown in panel e, initiated by 5 nM input. (j) Average count of localizations per μm fiber as a function of input concentration. Error bars represent standard deviation.

the alternated assembly of two metastable hairpins, triggered by a single stranded input. First, an input oligonucleotide (**input**) binds to toehold **a′** on the first hairpin (H1) and subsequently opens the stem of the hairpin, hereby activating toehold **b′**.

DOI: 10.1021/jacs.8b06146
J. Am. Chem. Soc. 2018, 140, 9758−9767

Next, the second hairpin (H2) binds to **b′** and is opened via branch migration to activate toehold **a**. Consequently, a new H1 can bind, resulting in the linear growth of an assembly of alternating hairpins. As the formed oligomer is connected to the initiator, which is typically the analyte, HCR has proven to be particularly useful for signal amplification in imaging of single nucleic acid molecules.[51,52] However, readout is time-consuming, especially when the HCR hairpins are kept at low nM concentration.

In order to template the HCR on the supramolecular BTA polymer scaffold, the sequence of H1 as reported by Pierce and co-workers was elongated with the 10 nucleotide antihandle sequence.[47] Consequently, the opening of H1 by the growing assembly is templated by the supramolecular polymer, which should increase the overall kinetics. In order to monitor the HCR in real-time, H1 was internally modified with a Cy3 fluorophore and H2 was modified with a Cy5 at its 5′ end, resulting in an increase in FRET from Cy3 to Cy5 upon assembly of the oligomer (Figure 4a). Additionally, H2 freely diffuses in solution and is only recruited to the BTA polymer via the growing assembly, allowing formation of the HCR-product to be visualized using fluorescence microscopy. First, the influence of the concentration of the supramolecular polymer on the performance of the templated HCR was evaluated. To this end, the HCR was monitored in time directly after adding 10 nM input to a preincubated mixture containing various concentrations of BTA polymer composed of 10% BTA-DNA, 50 nM H1, and 200 nM H2. A large excess of H2 was added to make sure that the opening of H2 by H1 is not rate limiting. Figure 4b shows that in absence of the polymer scaffold the HCR is slow, resulting in a yield of only 30% after 3 h incubation. In the presence of sufficiently high concentrations of supramolecular polymer, the HCR is strongly accelerated and reaches full conversion within 1 h. Both the rate and the final yield of the BTA templated HCR are clearly dependent on the concentration of supramolecular polymer. Similar to the supramolecular polymer templated multi-input AND gates, this can be explained by a trade-off between a sufficiently large polymer surface to accommodate all HCR products and the inversely correlated effective concentration of the HCR reactants recruited to the supramolecular polymer, with an optimal BTA concentration of 5 μM. Similar to the CHA reaction, optimal performance of the HCR reaction was observed using 5−10% BTA-DNA, with higher BTA-DNA to BTA ratios resulting in lower yields (Figure S7).

Having determined the optimal polymer concentration, next the concentration of input oligonucleotide was varied using a preincubated mixture containing 5 μM BTA polymer composed of 10% BTA-DNA, 50 nM H1, and 200 nM H2 (Figure 4c). No product is formed in the absence of input, confirming the stability of both hairpins and the absence of background activation. Upon the addition of increasing amounts of input, a clear increase in reaction yield is observed. Notably, when the input concentration exceeds 10 nM, the final emission ratio decreases. This effect is due to the formation of increasing amounts of smaller HCR products of which the donor of the initial H1 in the assembly is not neighboring an acceptor fluorophore. Interestingly, at low input concentrations (<10 nM), the final yield of the HCR is dependent on the input concentration. As the input concentrations should only determine the amount and the inversely correlated length of the assembled product, this result is counterintuitive. This input dependency could originate from two phenomena. First, malformed hairpins resulting from spurious synthesis errors and/or misfolding could act as chain stoppers that terminate the growth of the assembly. These effects become more dominant when less, but larger assemblies are formed.[53,54] Second, when templated by the BTA polymer, the length of the HCR assembly could be dictated by the length and/or structural characteristics of the polymer scaffold itself. In other words, at low input concentrations the amount of input may not be sufficient to trigger the HCR on all polymer fibers.

To study the dependency of the HCR reaction on the input concentration in more detail, the reaction products from the experiments shown in Figure 4c were analyzed using super-resolution fluorescence microscopy. Initial attempts to immobilize the supramolecular assemblies on a glass substrate via physical adsorption resulted in high background signals due to nonspecific adsorption of H2. To avoid this background binding, the glass substrate was passivated by coating with BSA-biotin conjugates, subsequently allowing the coverslip to be functionalized with the antihandle sequence by sequentially flowing streptavidin and the biotin-functionalized antihandle sequence in the flow-chamber (Figure S8). The BTA polymers decorated with the assembled HCR products could thus be selectively recruited to the coverslip surface via vacant BTA-DNA monomers present in the supramolecular polymer. As H1 is hybridized to the supramolecular polymer both in the absence and presence of the HCR, we used the Cy3 channel to image the BTA polymer backbone. Figure 4d shows the Cy3 channel of BTA polymers with the HCR triggered by different concentrations of input imaged by total internal reflection microscopy (TIRF). Micrometer-long fibrous structures are clearly resolved with little background signal, irrespective whether the HCR is triggered, showing that immobilized BTA polymers on the coverslip retain their overall polymeric morphology. Next, to visualize the formed HCR products at high resolution, the Cy5 channel (i.e., H2 in HCR product) was imaged using stochastic optical reconstruction microscopy (STORM). Figure 4e shows the STORM analysis of the same region of interest as shown in Figure 4d. In absence of input, no Cy5 localizations are observed, confirming that no HCR products are formed. When initiated by the input oligonucleotide, fibrous structures are resolved that superimpose with the BTA polymer observed in the Cy3 channel, which confirms that the HCR reaction is indeed templated by the supramolecular BTA polymer. To determine whether the length of the HCR products is physically limited by the length of the supramolecular polymer template, the STORM images were analyzed using a previously reported custom-made Matlab script.[40] This script traces individual BTA polymer backbones and subsequently determines the density of Cy5 localizations along the polymer scaffold. Figure 4f−i shows the traced polymer backbone and corresponding density of Cy5 localizations along the polymer for the boxed fibers in Figure 4e, initiated by 1 or 5 nM input, respectively. When initiated by 1 nM input, the fiber contains multiple, individual clusters of localizations of ∼250 nm in length. When the HCR is initiated by 5 nM input, the Cy5 fluorescence becomes continuous along the entire fiber and individual clusters can no longer be observed (Figure 4h,i). Finally, analysis of multiple fibers reveals a clear increase in the number of localizations per μm fiber at increasing input concentrations, up to an input concentration of 5 nM (Figure 4j). In conclusion, the observation of short clusters when triggered by low concentrations of input suggests that the length of the HCR products is not physically limited by the length of the supramolecular polymers. The input dependency

DOI: 10.1021/jacs.8b06146
J. Am. Chem. Soc. 2018, 140, 9758−9767

may therefore be due to the presence of a minor portion of malformed hairpins that terminate the growth of the assembly or the presence of assembly defects in the supramolecular polymer that result in kinetically trapped HCR assemblies.

CONCLUSION

In this work, we established the use of DNA-decorated supramolecular polymers as an attractive scaffold for DNA-based molecular computing. Recruitment of DNA reagents on the BTA polymer resulted in a large increase of effective concentration, which accelerated strand displacement reactions by 2 orders of magnitude. In addition to this kinetic effect, stabilization of the reaction products by multivalent interactions with the supramolecular polymer also increased the thermodynamic driving force for strand exchange reactions. The general applicability of the BTA-DNA scaffold to increase the speed and efficiency of DNA-based computing was demonstrated for multi-input AND gates and two well-established signal amplification strategies, CHA and HCR. The implementation of the supramolecular BTA polymer platform only required the elongation of DNA reactants with a complementary antihandle sequence, without any further sequence optimization. It is important to realize that, in contrast to recruitment on DNA origami templates, the DNA components are not sequentially aligned on the scaffold, but will be randomly recruited on the scaffold. Our finding that DNA computing is nonetheless efficiently templated, can be explained by the fact that the interaction between the handle ($\mathbf{x}'$) and the antihandle strand ($\mathbf{x}$) is highly dynamic and readily reversible with a predicted dissociation rate of $\sim$1 s^{-1}.[55] This dynamic recruitment is thus essential for the effectiveness of the system, as it allows enhancement of the effective rates by increasing the effective local concentration of the DNA components, without having to "program" the exact order of the different DNA components on the scaffold. The supramolecular nature of the BTA polymer allowed the scaffold composition to be easily optimized for each application, making our approach also applicable to other DNA-based computing system that are based on freely diffusing oligonucleotide reactants. In the present system, exchange of BTA monomers is relatively slow (2−3 h), and the exchange of DNA reactants is therefore determined by rapid association and dissociation of the 10 nucleotide antihandle on the BTA-DNA backbone. Increasing the monomer exchange rates may allow the system to adapt the local density of DNA-handle strands during DNA computation, which might increase the ability of the system to cope with assembly defects.[41]

Performing isothermal amplification reactions such as CHA and HCR on BTA polymers may have other advantages besides increasing their speed. E.g., so far catalytic hairpin assembly has not been applied for signal amplification in single-molecule imaging, because the generated fluorescence diffuses away from the analyte. However, when templated the activated reporter is anchored to the supramolecular polymer and the fluorescent signal remains associated with the target. In this manner, CHA could be used as an alternative to HCR for the amplification of immunosignals both in immune-assays and in antibody-mediated fluorescence imaging.[52] In this study, we employed well-established, classical designs for both the CHA and HCR reactions, but further rate enhancements can probably be achieved by adopting new and improved sequence designs.[56] Optimization of the hairpin sequences specifically for templated reactions may further increase the amplification speed, in particular for the CHA reaction. The CHA system used in this study contained an 8 nucleotide long toehold for the catalyst binding to H1, which may have slowed-down release of the catalyst from the intermediate ternary complex and thus limited the turnover number of the CHA. The templated CHA reaction could thus be further optimized by changing the size of this toehold or by tuning the affinity between the catalyst antihandle and the BTA-DNA handle to ensure efficient recruitment of the catalyst to the polymer, while also allowing rapid dissociation from the intermediate complex.

In addition to their application in signal amplification, DNA-functionalized BTA polymers may also be used to construct autonomous systems that are able to detect external inputs and release molecular cargo, controlled by templated DNA-based molecular circuits. In these applications, the BTA-DNA scaffold would not only enhance the computational speed but also act to confine and efficiently integrate various DNA-based modules developed for signal detection, signal processing and ligand release.[57−59] Many applications of such systems can be envisioned, including the development of responsive biomaterials and smart drug delivery systems. Moreover, because the BTA polymer has already been demonstrated to efficiently transfect RNA into cells,[60] BTA-DNA-confined systems could be integrated with intracellular signaling pathways and programmed to interact with and control endogenous RNA and protein activities.

EXPERIMENTAL SECTION

Chemicals and Reagents. Solvents and reagents were purchased from commercial sources and used without further purification. The alkyne functionalized handle oligonucleotide was purchased from Base Click GmbH. All other oligonucleotides were obtained HPLC purified from Integrated DNA Technologies and dissolved upon arrival in TE buffer (10 mM Tris−HCl, 1 mM EDTA at pH 8.0). The concentration was determined by UV−vis and the extinction coefficients specified by the manufacturer, after which the oligonucleotides were further diluted to a stock concentration of 50 μM and stored at −30 °C.

The handle-functionalized BTA monomer (BTA-DNA) was synthesized as described previously.[38] The supramolecular polymers were assembled by drying an appropriate amount of BTA-3OH in a glass vial under vacuum. Subsequently, an appropriate amount of BTA-DNA dissolved in water was added and the solution was stirred for 15 min at 80 °C. Finally, the solutions were vortexed for 15 s and allowed to equilibrate at room temperature overnight.

Assembly of DNA-Circuit Components. All multi-input AND gates were assembled by mixing 2.5 μM of fluorescent base strand with 3 μM of all blocking strands in TAE/Mg^{2+} (40 mM Tris−HCl, 20 mM acetic acid, 2 mM EDTA, 12.5 mM magnesium acetate at pH 8.0.) and annealed from 90 to 15 °C in 1 h. Similarly, complex X for the strand displacement and strand exchange reactions was obtained by annealing 2.5 μM of both strands in TAE/Mg^{2+} from 90 to 15 °C in 1 h. All hairpin forming oligonucleotides for the HCR and CHA were diluted in TAE/Mg^{2+} to a final concentration of 2.5 μM and annealed from 90 to 15 °C in 1 h. From these stock solutions, fresh dilutions were made in TAE/Mg^{2+} supplemented with 1 mg mL^{-1} BSA or TNaK buffer (20 mM Tris−HCl, 140 mM NaCl, 5 mM KCl at pH 7.5) supplemented with 1 mg mL^{-1} BSA.

Fluorescence Kinetics Characterization. All kinetic experiments were performed in a 384 well plate with a final volume of 50 μL and measured with a Tecan infinite 500 plate reader equilibrated at 25 °C (or 37 °C for CHA). The strand displacement reactions were measured at 30 s intervals with a fixed gain and λ_{ex} = 485 nm and λ_{em} = 520 nm. The obtained fluorescence intensities were normalized to concentration of displaced output using a calibration curve where various amounts of fully complementary input were incubated with 20 nM complex X, showing a linear correlation between generated fluorescence and input concentration (Supporting Information). The multi-input AND gates were measured at 5 min intervals with a fixed

DOI: 10.1021/jacs.8b06146
J. Am. Chem. Soc. 2018, 140, 9758−9767

gain and λ_{ex} = 485 nm and λ_{em} = 520 nm. Control experiments for the 4-input AND gate were done by leaving out one of the four input strands. The CHA was measured at 1 min intervals with λ_{ex} = 485 nm and λ_{em} = 520 nm. In addition to the control without BTA, a second control was done using 5 μM inert BTA polymer and 500 nM nonconjugated handle. HCR was monitored by measuring the ratio of the Cy5 ($\lambda_{em,Cy5}$ = 670 nm) and Cy3 ($\lambda_{em,Cy3}$ = 590 nm) emissions while exciting at λ_{ex} = 535 nm.

Super Resolution Microscopy. The flow chamber for fluorescence microscopy was prepared similar to previous reports for super resolution imaging of DNA origami structures.[61] In short, a flow chamber was constructed by adhering a glass microscope coverslip (Menzel-Gläser, no. 21 × 26 mm) to a glass slide separated by double-sided tape. Next, 25 μL of 0.5 mg mL^{-1} BSA-biotin (Thermo Fisher) in buffer A (10 mM Tris−HCl, 100 mM NaCl, and 0.05% (v/v) Tween 20 at pH 8.0) was flown in the chamber and incubated for 5 min. Subsequently, the flow chamber was washed with 40 μL buffer A and 25 μL of a 0.5 mg mL^{-1} streptavidin (in buffer A) was added and incubated for 2 min. After washing with buffer A and buffer B (5 mM Tris−HCl, 10 mM $MgCl_2$, 1 mM EDTA, and 0.05% (v/v) Tween 20 at pH 8.0), 25 μL of a 100 nM antihandle-biotin solution in buffer A was flown in the chamber and incubated for 2 min. Finally, after washing with 40 μL buffer A and 40 μL buffer B, 25 μL sample was flown in the chamber and incubated for 2 min. Before TIRF and STORM analysis, the flow chamber was washed with 40 μL of imaging buffer (50 mM Tris−HCl pH 7.0, and oxygen scavenging system (0.5 mg mL^{-1} glucose oxidase, 50 μg mL^{-1} catalase), 10% (w/vol) glucose, and 10 mM 2-aminoethanethiol). STORM and TIRF images were acquired with a Nikon N-STORM system. Cy3 and Cy5 were excited using a 561 and 647 nm laser, respectively. Fluorescence was collected by means of a Nikon x100, 1.4NA oil immersion objective and passed through a quad-band-pass dichroic filter (97335 Nikon). Images were recorded with an EMCCD camera (ixon3, Andor, pixel size 0.165 μm). The movies were subsequently analyzed with the STORM module of the NIS element Nikon software. The localizations generated by the Nikon software were subsequently analyzed using a previously described custom-made Matlab script.[40]

■ ASSOCIATED CONTENT

Supporting Information

The Supporting Information is available free of charge on the ACS Publications website at DOI: 10.1021/jacs.8b06146.

Oligonucleotide sequences, visual DSD fitting of diffusive and templated strand displacement reactions, detailed AND-gate characterization, secondary structure analysis of the CHA catalyst, CHA and HCR kinetics at various BTA-DNA densities, and overview of immobilization strategy for DNA-decorated supramolecular BTA polymers (PDF)

■ AUTHOR INFORMATION

Corresponding Author

*m.merkx@tue.nl

ORCID

Maarten Merkx: 0000-0001-9484-3882

Notes

The authors declare no competing financial interest.

■ ACKNOWLEDGMENTS

We thank C. M. A. Leenders for the synthesis of BTA-DNA. E. W. Meijer is gratefully acknowledged for valuable insights and fruitful discussions. This work was supported by funding from the Ministry of Education, Culture and Science (Gravity program, 024.001.035), and a European Research Council (ERC) Starting Grant (280255).

■ REFERENCES

(1) Chen, Y.-J.; Groves, B.; Muscat, R. A.; Seelig, G. *Nat. Nanotechnol.* **2015**, *10*, 748−760.
(2) Srinivas, N.; Parkin, J.; Seelig, G.; Winfree, E.; Soloveichik, D. *Science* **2017**, *358*, eaal2052.
(3) Padirac, A.; Fujii, T.; Estévez-Torres, A.; Rondelez, Y. *J. Am. Chem. Soc.* **2013**, *135*, 14586−14592.
(4) Douglas, S. M.; Bachelet, I.; Church, G. M. *Science* **2012**, *335*, 831−834.
(5) Thubagere, A. J.; Li, W.; Johnson, R. F.; Chen, Z.; Doroudi, S.; Lee, Y. L.; Izatt, G.; Wittman, S.; Srinivas, N.; Woods, D.; Winfree, E.; Qian, L. *Science* **2017**, *357*, eaan6558.
(6) Shin, J.-S.; Pierce, N. A. *J. Am. Chem. Soc.* **2004**, *126*, 10834−10835.
(7) Sherman, W. B.; Seeman, N. C. *Nano Lett.* **2004**, *4*, 1203−1207.
(8) Jung, C.; Allen, P. B.; Ellington, A. D. *Nat. Nanotechnol.* **2016**, *11*, 157−163.
(9) Yurke, B.; Turberfield, A. J.; Mills, A. P.; Simmel, F. C.; Neumann, J. L. *Nature* **2000**, *406*, 605−608.
(10) Chen, Y.; Lee, S.-H.; Mao, C. *Angew. Chem., Int. Ed.* **2004**, *43*, 5335−5338.
(11) Seelig, G.; Soloveichik, D.; Zhang, D. Y.; Winfree, E. *Science* **2006**, *314*, 1585−1588.
(12) Zhang, D. Y.; Turberfield, A. J.; Yurke, B.; Winfree, E. *Science* **2007**, *318*, 1121−1125.
(13) Qian, L.; Winfree, E.; Bruck, J. *Nature* **2011**, *475*, 368−372.
(14) Qian, L.; Winfree, E. *Science* **2011**, *332*, 1196−1201.
(15) Chen, Y.-J.; Dalchau, N.; Srinivas, N.; Phillips, A.; Cardelli, L.; Soloveichik, D.; Seelig, G. *Nat. Nanotechnol.* **2013**, *8*, 755−762.
(16) Groves, B.; Chen, Y.-J.; Zurla, C.; Pochekailov, S.; Kirschman, J. L.; Santangelo, P. J.; Seelig, G. *Nat. Nanotechnol.* **2016**, *11*, 287−294.
(17) Good, M. C.; Zalatan, J. G.; Lim, W. A. *Science* **2011**, *332*, 680−686.
(18) Pawson, T.; Scott, J. D. *Science* **1997**, *278*, 2075−2080.
(19) Idan, O.; Hess, H. *ACS Nano* **2013**, *7*, 8658−8665.
(20) Jung, C.; Allen, P. B.; Ellington, A. D. *ACS Nano* **2017**, *11*, 8047−8054.
(21) You, M.; Lyu, Y.; Han, D.; Qiu, L.; Liu, Q.; Chen, T.; Wu, C. S.; Peng, L.; Zhang, L.; Bao, G.; Tan, W. *Nat. Nanotechnol.* **2017**, *12*, 453−459.
(22) Rudchenko, M.; Taylor, S.; Pallavi, P.; Dechkovskaia, A.; Khan, S.; Butler, V. P., Jr.; Rudchenko, S.; Stojanovic, M. N. *Nat. Nanotechnol.* **2013**, *8*, 580−586.
(23) Muscat, R. A.; Strauss, K.; Ceze, L.; Seelig, G. In *Proceedings of the 40th Annual International Symposium on Computer Architecture*; ISCA '13; ACM: New York, NY, USA, 2013; pp 177−188.
(24) Mullor Ruiz, I.; Arbona, J.-M.; Lad, A.; Mendoza, O.; Aimé, J.-P.; Elezgaray, J. *Nanoscale* **2015**, *7*, 12970−12978.
(25) Bui, H.; Shah, S.; Mokhtar, R.; Song, T.; Garg, S.; Reif, J. *ACS Nano* **2018**, *12*, 1146−1155.
(26) Bui, H.; Miao, V.; Garg, S.; Mokhtar, R.; Song, T.; Reif, J. *Small* **2017**, *13*, 1602983.
(27) Chatterjee, G.; Dalchau, N.; Muscat, R. A.; Phillips, A.; Seelig, G. *Nat. Nanotechnol.* **2017**, *12*, 920−927.
(28) Li, J.; Johnson-Buck, A.; Yang, Y. R.; Shih, W. M.; Yan, H.; Walter, N. G. *Nat. Nanotechnol.* **2018**, DOI: 10.1038/s41565-018-0130-2.
(29) Helmig, S.; Gothelf, K. V. *Angew. Chem., Int. Ed.* **2017**, *56*, 13633−13636.
(30) Tomov, T. E.; Tsukanov, R.; Liber, M.; Masoud, R.; Plavner, N.; Nir, E. *J. Am. Chem. Soc.* **2013**, *135*, 11935−11941.
(31) Strauss, M. T.; Schueder, F.; Haas, D.; Nickels, P. C.; Jungmann, R. *Nat. Commun.* **2018**, *9*, 1600.
(32) Milligan, J. N.; Ellington, A. D. *Chem. Commun.* **2015**, *51*, 9503−9506.
(33) Shimada, N.; Saito, K.; Miyata, T.; Sato, H.; Kobayashi, S.; Maruyama, A. *Adv. Funct. Mater.* **2018**, *28*, 1707406.
(34) Kim, W. J.; Akaike, T.; Maruyama, A. *J. Am. Chem. Soc.* **2002**, *124*, 12676−12677.

DOI: 10.1021/jacs.8b06146
J. Am. Chem. Soc. 2018, 140, 9758−9767

(35) Alemán García, M. Á.; Magdalena Estirado, E.; Milroy, L.-G.; Brunsveld, L. *Angew. Chem., Int. Ed.* **2018**, *57*, 4976−4980.
(36) Vyborna, Y.; Vybornyi, M.; Häner, R. *Chem. Commun.* **2017**, *53*, 5179−5181.
(37) Noteborn, W. E. M.; Saez Talens, V.; Kieltyka, R. E. *ChemBioChem* **2017**, *18*, 1995−1999.
(38) Wijnands, S. P. W.; Engelen, W.; Lafleur, R. P. M.; Meijer, E. W.; Merkx, M. *Nat. Commun.* **2018**, *9*, 65.
(39) Leenders, C. M. A.; Albertazzi, L.; Mes, T.; Koenigs, M. M. E.; Palmans, A. R. A.; Meijer, E. W. *Chem. Commun.* **2013**, *49*, 1963−1965.
(40) Albertazzi, L.; van der Zwaag, D.; Leenders, C. M. A.; Fitzner, R.; van der Hofstad, R. W.; Meijer, E. W. *Science* **2014**, *344*, 491−495.
(41) Lou, X.; Lafleur, R. P. M.; Leenders, C. M. A.; Schoenmakers, S. M. C.; Matsumoto, N. M.; Baker, M. B.; van Dongen, J. L. J.; Palmans, A. R. A.; Meijer, E. W. *Nat. Commun.* **2017**, *8*, 15420.
(42) Zhang, D. Y.; Winfree, E. *J. Am. Chem. Soc.* **2009**, *131*, 17303−17314.
(43) Dalchau, N.; Chandran, H.; Gopalkrishnan, N.; Phillips, A.; Reif, J. *ACS Synth. Biol.* **2015**, *4*, 898−913.
(44) Moreira, B. G.; You, Y.; Behlke, M. A.; Owczarzy, R. *Biochem. Biophys. Res. Commun.* **2005**, *327*, 473−484.
(45) Yin, P.; Choi, H. M. T.; Calvert, C. R.; Pierce, N. A. *Nature* **2008**, *451*, 318−322.
(46) Li, B.; Ellington, A. D.; Chen, X. *Nucleic Acids Res.* **2011**, *39*, e110−e110.
(47) Dirks, R. M.; Pierce, N. A. *Proc. Natl. Acad. Sci. U. S. A.* **2004**, *101*, 15275−15278.
(48) Choi, H. M. T.; Chang, J. Y.; Trinh, L. A.; Padilla, J. E.; Fraser, S. E.; Pierce, N. A. *Nat. Biotechnol.* **2010**, *28*, 1208−1212.
(49) Cheglakov, Z.; Cronin, T. M.; He, C.; Weizmann, Y. *J. Am. Chem. Soc.* **2015**, *137*, 6116−6119.
(50) Bi, S.; Yue, S.; Zhang, S. *Chem. Soc. Rev.* **2017**, *46*, 4281−4298.
(51) Choi, H. M. T.; Beck, V. A.; Pierce, N. A. *ACS Nano* **2014**, *8*, 4284−4294.
(52) Lin, R.; Feng, Q.; Li, P.; Zhou, P.; Wang, R.; Liu, Z.; Wang, Z.; Qi, X.; Tang, N.; Shao, F.; Luo, M. *Nat. Methods* **2018**, *15*, 275−278.
(53) Chen, X.; Briggs, N.; McLain, J. R.; Ellington, A. D. *Proc. Natl. Acad. Sci. U. S. A.* **2013**, *110*, 5386−5391.
(54) Zhang, D. Y.; Winfree, E. *Nucleic Acids Res.* **2010**, *38*, 4182−4197.
(55) Jungmann, R.; Steinhauer, C.; Scheible, M.; Kuzyk, A.; Tinnefeld, P.; Simmel, F. C. *Nano Lett.* **2010**, *10*, 4756−4761.
(56) Ang, Y. S.; Yung, L.-Y. L. *Chem. Commun.* **2016**, *52*, 4219−4222.
(57) Janssen, B. M. G.; van Rosmalen, M.; van Beek, L.; Merkx, M. *Angew. Chem., Int. Ed.* **2015**, *54*, 2530−2533.
(58) Engelen, W.; Janssen, B. M. G.; Merkx, M. *Chem. Commun.* **2016**, *52*, 3598−3610.
(59) Engelen, W.; Meijer, L. H. H.; Somers, B.; de Greef, T. F. A.; Merkx, M. *Nat. Commun.* **2017**, *8*, 14473.
(60) Bakker, M. H.; Lee, C. C.; Meijer, E. W.; Dankers, P. Y. W.; Albertazzi, L. *ACS Nano* **2016**, *10*, 1845−1852.
(61) Schnitzbauer, J.; Strauss, M. T.; Schlichthaerle, T.; Schueder, F.; Jungmann, R. *Nat. Protoc.* **2017**, *12*, 1198−1228.

DOI: 10.1021/jacs.8b06146
J. Am. Chem. Soc. 2018, 140, 9758−9767